Superconductor Science and Technology

PAPER

Network modeling of non-ideal superconducting resonator circuits

IOP Publishing Superconductor Science and Technology
Supercond. Sci. Technol. **33** (2020) 075004 (7pp) https://doi.org/10.1088/1361-6668/ab89eb

Network modeling of non-ideal superconducting resonator circuits

H Guan[1], M Dai[2], Q He[2], J Hu[1], P Ouyang[2], Y Wang[1], L F Wei[2] and J Gao[3]

[1] Quantum Optoelectronics Laboratory, School of Physical Science and Technology, Southwest Jiaotong University, Chengdu, 610031, People's Republic of China
[2] Information Quantum Technology Laboratory, School of Information Science and Technology, Southwest Jiaotong University, Chengdu, 610031, People's Republic of China
[3] National Institute of Standards and Technology, Boulder, CO 80305, United States of America

E-mail: yiwenwang.nju@gmail.com and weilianfu@gmail.com

Received 1 December 2019, revised 6 March 2020
Accepted for publication 16 April 2020
Published 13 May 2020

Abstract

We originally develop a network analysis method to study the non-ideal superconducting resonator circuits. We model the resonator device by a 3-block serial network, consisting of input feedline, resonator-coupler and output feedline. We show that the resonance curve will be modified if non-negligible discontinuity (reflection) exists at input or output side of the resonator. The extracted resonance parameters (such as coupling quality factor Q_c) from only fitting the transmission deviate from their true values as originally defined in matched impedance conditions, and the deviation depends on a single parameter which includes all the non-ideal effects from the circuits. We prove that the internal quality factor Q_i can be accurately extracted from the modified transmission curve by using a very simple graphical method. Our methods and results are quantitatively verified by both simulations and experiments on superconducting microstrip resonators. Comparing to the usual circuit analysis, our network analysis method is more intuitive and easier to understand. It can serve as a general tool to study the non-ideal superconducting resonator circuits.

Keywords: superconducting resonator, superconducting circuits, kinetic inductance detector, network analysis, quality factor, impedance mismatching

(Some figures may appear in colour only in the online journal)

1. Introduction

Superconducting micro-resonators [1] have been widely used in many frontier research fields, such as photon detection [2], superconducting quantum computing [3, 4], and quantum-limited parametric amplifiers [5, 6]. In all these applications, it is necessary to understand the resonance circuit and accurately determine the resonance parameters, particularly the quality factor. For example, microwave kinetic inductance detectors (MKIDs) [7, 8] are pair-breaking photon detectors based on high-quality (high-Q) superconducting thin-film micro-resonators. For MKIDs, the coupling quality factor (Q_c), which describes the coupling strength of the resonator and the feedline, is typically designed to be an appropriate value (about $10 \times 10^3 \sim 40 \times 10^3$) for optimizing the detector responsivity and dynamical range [9]. On the other hand, the internal quality factor (Q_i) describes the intrinsic losses. Q_i is required to be as high as possible (normally above $10^5 \gg Q_c$), and thus the total Q is usually limited by Q_c. Q_i is mainly dependent on the substrate and the superconducting material of choice [10–12]. Precise measurements of Q_i with temperature, microwave power and optical illumination are important tools to reveal the microscopic loss mechanisms and study the dynamics of non-equilibrium quasi-particles in the device [13–19].

Although there are many circuit models and fitting techniques discussed in literature [20–22] for extracting important resonator parameters, non-ideal electronic circuits can lead to an asymmetry in the complex transmissions [19, 23], which complicates the interpretation and determination of Q_i and Q_c. Reference [23] presents a circuit analysis method, showing how asymmetry in the resonance line shape can arise from

coupling the resonator to mismatched input and output transmission impedance. The authors propose a diameter correction method (DCM) for extracting an accurate Q_i. DCM is superior to the widely used rotation method [15, 24, 25], which simply adds an empirical rotation to the resonance circle and may overestimate Q_i.

In this paper, we describe a network analysis method, which is more intuitive and easier to understand comparing to the usual circuit analysis method [19, 23], to study the non-ideal superconducting resonator circuits. The non-ideal circuit effects are mainly from the impedance mismatched transmission line, therefore we model the resonator device by a 3-block serial network: the input feedline, the resonator-coupler and the output feedline. It shows that if non-negligible discontinuity (reflection) exists at input or output side of the resonator, the resonance curve will be modified from its original shape and become asymmetric. The total quality factor Q, coupling quality factor Q_c and resonance frequency f_r extracted from only fitting the complex transmission data (S_{21}) deviate from their true values in the matched impedance conditions. We find that the deviation scales with a single parameter which accounts for all the non-ideal effects from the feedline. Besides, we prove that the internal quality factor Q_i can be accurately obtained from the modified transmission curve by using a very simple graphical method, which is essentially the same as DCM but easier to implement. Our results are quantitatively verified by both simulations and experiments on superconducting microstrip resonators.

2. Network analysis method

We first consider a simple resonator-coupler's 2-port network (as shown in figure 1(a)), where a resonator is coupled to a lossless 50 ohm transmission line and the two ports are both impedance matched ports. It can be derived that the transmission (as a function of frequency) through this resonator-coupler's 2-port network (after removing the cable delay effects of the transmission line) is [26, 27]

$$S_{21}(f) = S_{12}(f) = 1 - \phi(f) \tag{1}$$

and

$$\phi(f) = \frac{Q/Q_c}{1 + 2jQ(\frac{f-f_r}{f_r})} \tag{2}$$

where we define Q, Q_c, Q_i and f_r as the true values of the total quality factor, coupling quality factor, internal quality factor and resonance frequency respectively. For an ideal resonator-coupler block with matched impedance, one can easily obtain the true values of resonance parameters by fitting equation (1). Note that equation (1) holds for weak feedline-resonator coupling limit ($Q_c \gg 1$) [27], which is well satisfied in the usual MKID applications. Q, Q_c and Q_i are connected by the relation $1/Q = 1/Q_c + 1/Q_i$. One can also obtain the reflection of this resonator-coupler's 2-port network:

$$S_{11} = S_{22} = \phi \tag{3}$$

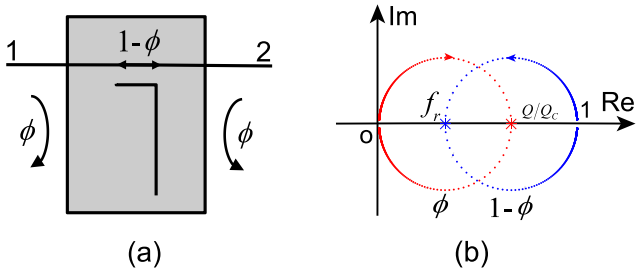

Figure 1. (a) The ideal resonator-coupler's 2-port network. A resonator is coupled to a 50 ohm feedline and the impedance of both ports is also 50 ohm. (b) The original reflection curve ϕ (red) and transmission curve (blue) in complex plane. The arrow shows the direction of increasing frequency.

As shown in figure 1(b), ϕ defines a circle (red) in the complex plane, with its off-resonance point at origin $\phi(f=\infty) = 0$, on-resonance point on the positive x-axis $\phi(f=f_r) = Q/Q_c$ and the diameter being $d = Q/Q_c$. Therefore the transmission curve $S_{21} = 1 - \phi$ shows the same circle but flipped and translated, as shown by the blue curve in figure 1(b). Hereafter we call this curve the original resonance (transmission) curve, which has the feature that the circle is 'facing the origin', i.e. the line connecting the off-resonance point and on-resonance point extends to the origin. Therefore the original resonance curve is symmetric.

Now we consider a real resonator device, which is shown in figure 2(a). The resonator chip is glued onto a gold plated copper box with two 50 ohm SMA connectors. The center pin of each connector is soldered to the feedline on a printed circuit board (PCB), which is designed to have a characteristic impedance of 50 ohm. The feedline on the chip, which is also designed to be of 50 ohm impedance, is connected to the PCB feedline by a few Aluminum (Al) wires of 25 μm in diameter and typically 2 ~ 6 mm in length. If the feedline before and after the resonator is a perfect transmission line and impedance is matched everywhere, one will obtain the original resonance curve when measuring the transmission of the device with a vector network analyzer (VNA), but we usually get a distorted resonance curve in experiments. An obvious feature of the distorted curve is that the circle is not always 'facing the origin' (see figure 3(a)). To understand this and some other features, we have to take the non-ideal effects of the feedline into consideration, i.e. the impedance is not matched everywhere on the feedline thus the reflection at input side or output side of the resonator is not negligible.

As shown in figure 2(a), we divide the whole device box into three blocks (from left to right): input feedline block (from the coaxial input port to before the resonator), the resonator-coupler block, and output feedline block (from after the resonator to the coaxial output port). The three blocks are in serial connection and each block is modeled by a reciprocal 2-port network element, with transmission and reflection coefficients shown in figure 2(b). The transmission coefficients of input (output) feedline block are t_1 (t_2), and the reflection coefficients are r_1 and r_1' (r_2' and r_2). Note that r_1 and r_1' (r_2' and r_2) differ by a finite phase. Strictly speaking, these coefficients

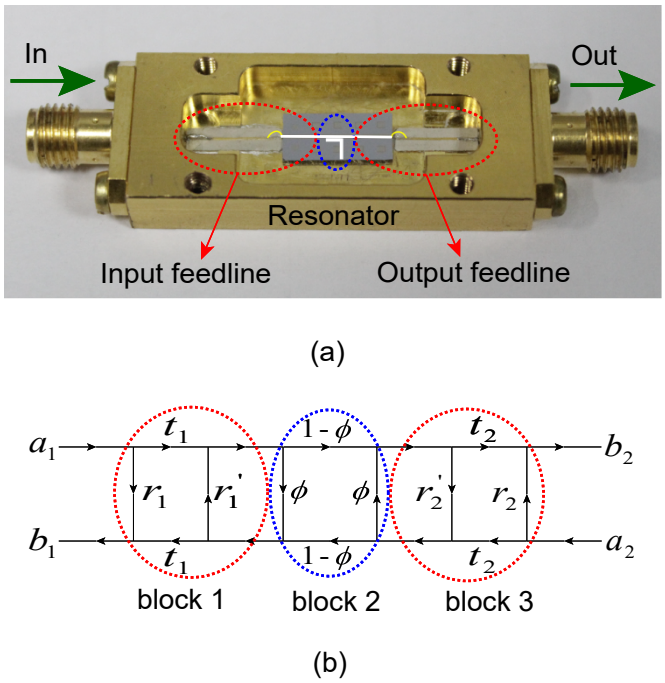

Figure 2. (a) Real device modeled by a 3-block serial network. The white line represents the on-chip feedline and resonator. The yellow lines represent the bonding wires. (b) Block diagram and signal flow graph with transmission (reflection) coefficients for all branches, which are used to calculate the total transmission and reflection of the whole device.

are frequency dependent. Here we assume that in the narrow frequency bandwidth of resonance they are flat enough to be taken as constants. In figure 2(b), we also construct a signal flow graph, which can give an intuitive graphical illustration of the microwave network behavior. The signal flow graph can then be reduced to a single branch between two nodes using some basic decomposition rules [28], and one can derive the desired wave amplitude ratios to calculate the *S*-parameters.

It can be derived (see appendix) that the total transmission S_{21} of the serial 3-block network is

$$S_{21} = \frac{t_1 t_2 (1-\phi)}{(1-r_1' r_2') + (-r_1' - r_2' + 2r_1' r_2')\phi} \tag{4}$$

Equation (4) can also be written in a compact form as

$$S_{21} = T\frac{1-\phi}{1+u\phi} \tag{5}$$

$$T = \frac{t_1 t_2}{1 - r_1' r_2'}$$
$$u = \frac{-r_1' - r_2' + 2r_1' r_2'}{1 - r_1' r_2'}$$

Physically speaking, T is the background transmission of the feedline in the absence of resonator and can be taken as a complex scaling factor which only scales and rotates the whole original resonance curve around the origin. If we normalize S_{21} by T, the original resonance curve will be modified from $1-\phi$ to $\frac{1-\phi}{1+u\phi}$. This is a bilinear transformation which will transform a circle (1 - ϕ) to another circle (the modified transmission curve). Here u is a complex number and the only parameter which includes all the non-ideal effects from the feedline on the resonance curve. After a little math, the normalized S_{21} can be reduced to a simple expression that is commonly used in references [24–26, 29]:

$$S_{21}' = \frac{S_{21}}{T} = 1 - \frac{\frac{Q/Q_c(1+u)}{1+u_r Q/Q_c}}{1 + \frac{2jQ(x+u_i/2Q_c)}{1+u_r Q/Q_c}} = 1 - \frac{Q'/Q_c' e^{j\theta}}{1+2jQ'x'} \tag{6}$$

where u_r (u_i) is the real (image) part of u and $x = \frac{f-f_r}{f_r}$. We also define a set of modified resonance parameters, which are related to their true values by:

$$Q' = \frac{Q}{1+u_r Q/Q_c} \tag{7}$$

$$Q_c' = \frac{Q_c}{|1+u|}$$
$$f_r' = f_r(1 - \frac{u_i}{2Q_c})$$

where Q' is the modified total quality factor, Q_c' is the modified coupling quality factor, f_r' is the modified resonance frequency, $x' = \frac{f-f_r'}{f_r'} = x + u_i/2Q_c$ and $1+u = |1+u|e^{j\theta}$ ($\theta = ang(1+u)$).

If we carry out the normal fitting procedures [26] on the measured transmission based on equation (6), we will get modified resonance parameters Q', Q_c', and f_r' instead of their true values and the deviation scales with the feedline parameter u. For perfect impedance matching, $u=0$, the modified resonance parameters go back to their true values. For non-negligible reflection at input or output side of the resonator ($r_1' \neq 0$ or $r_2' \neq 0$), u modifies the resonance parameters. Note that Q_c' can be higher or lower than Q_c, depending on the magnitude of $1/|1+u|$. The fractional resonance frequency shift is given by $(f_r' - f_r)/f_r = -u_i/2Q_c$. Because $u_i/2Q_c$ is quite small (on the order of the resonator's bandwidth), the resonance frequency will be shifted slightly (down or up depending on the sign of u_i). It can also be shown that the maximum wave amplitude inside the resonator occurs at f_r'.

From the modified transmission, we can also get the rotation angle θ, which describes a rotation of the resonance curve around the off-resonance point. Whenever u has a nonzero imaginary part, there will be a rotation and the resonance curve becomes asymmetric. Figure 3(a) shows the geometrical relation between the original resonance curve (with diameter Q/Q_c) and the modified resonance curve (with diameter Q'/Q_c'). The modified resonance curve and the real axis cross at point A, which is also the horizontal projection of the mod-

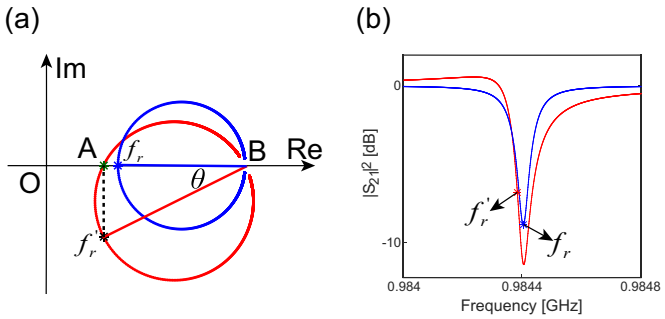

Figure 3. (a) The modified transmission curve (red circle) and original transmission curve (blue circle) in the complex plane. O is the origin, B is the off-resonance point, and A (green star) is the intersection of modified resonance curve and the real axis. f_r (blue star) and f_r' (black star) represent the on-resonance point of the original and modified resonance circle respectively. $|OB| = 1$ if we normalize both resonance curves to the background feedline transmission T, which does not affect the relative geometrical relations between these two resonance curves. θ is the rotation angle that the modified resonance circle rotates around B. (b) The original (symmetric) $|S_{21}|^2$ (blue) and modified (asymmetric) $|S_{21}|^2$ (red).

ified resonance point (f_r'). With the relations in equation (7), it can be easily derived that:

$$\frac{|OA|}{|OB|} = 1 - \frac{Q'}{Q_c'}\cos\theta = \frac{Q'}{Q_i} \tag{8}$$

This suggests that one can accurately extract the true internal quality factor Q_i from the modified transmission curve, by using normal fitting procedures to get Q' and then calculating as

$$Q_i' = \frac{|OB|}{|OA|}Q' = Q_i \tag{9}$$

Here, Q_i' is the extracted internal quality factor using the above graphical method, and in theory Q_i' should be equal to its true value Q_i. We want to emphasize that our graphical method is essentially equivalent to DCM. In both methods, one needs to firstly fit the same resonance circle to obtain the on-resonance point (f_r'), off-resonance point (B) and the total quality factor (Q'). However, our graphical method provides a direct connection between Q_i' and Q' (equation (9)), which is the simplest and most intuitive expression to obtain Q_i'. With graphical method, one can quickly obtain Q_i' by projecting on-resonance point (f_r') onto $|OB|$ to get the ratio $|OB|/|OA|$. For DCM, one needs to further determine the fitting parameters Q_c' and θ in order to calculate Q_i' by using the relation $1/Q_i' = 1/Q' - \cos\theta/Q_c'$. Although this relation in DCM is in theory equivalent to equation (9), our graphical method brings the ease of understanding and implementing in the determination of Q_i'.

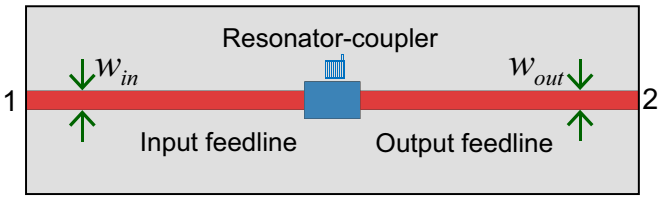

Figure 4. Schematics of the simulated 2-port microstrip resonator device, which can be divided into 3 blocks. The impedance of both ports are 50 ohm. The device is modeled as a single metal layer (with kinetic inductance 85 pH/sq) on 380 μm thick Silicon substrate (grey area). In the middle (blue), a lumped-element resonator is coupled to a short 470 μm wide transmission line with 50 ohm characteristic impedance. The gap between the resonator and the 50 ohm transmission line is fixed at 60 μm. The width of the input (output) feedline (red) is w_{in} (w_{out}), which can be adjusted to create various degrees of impedance mismatches. The lengths of input and output feedline are fixed at 15 mm in all simulations. The dissipation can be introduced and varied by tuning the dc sheet resistance R_{dc} of the metal layer.

3. Simulations

To test our 3-block network model and graphical method for extracting Q_i, we simulate the transmission of a 2-port superconducting microstrip resonator device using a numerical linear solver (Sonnet). As shown in figure 4, the 2-port resonator device consists of 3 serial blocks, which are input feedline block, middle resonator-coupler block, and output feedline block. We can simulate both the total transmission of the whole device and the transmission (reflection) of each block, so we are able to obtain the feedline parameter u, extract the true and modified resonance parameters, and then verify their relations (equation (7)).

We first study the effects of impedance mismatches. If we simulate only the middle resonator-coupler block, we will get a resonance frequency $f_r = 0.984\,405$ GHz, coupling quality factor $Q_c = 17.20 \times 10^3$, internal quality factor $Q_i = 121.94 \times 10^3$ and total quality factor $Q = 15.07 \times 10^3$. These are the true values of the resonance parameters because resonator-coupler block is impedance matched. We then create and adjust impedance mismatches by varying the width of input (output) feedline to change their characteristic impedance R_{in} (R_{out}). Table 1 lists the calculated u and extracted resonance parameters (Q_c', Q_i', f_r') under different impedance mismatching conditions. Note that in the real calculations of u, we have taken into account the effects of the finite length of the middle 50 ohm transmission line. For impedance matching (the width of input and output feedline is 470 μm) or slightly impedance mismatching conditions (the width of input and output feedline is 560 μm), $u \approx 0$ and the extracted resonance parameters are very close to their true values. If we increase the impedance mismatching level, u is not negligible, the extracted Q_c' and f_r' deviate from Q_c and f_r, which all quantitatively agree well with their relations (equation (7)) derived from the 3-block model. However, for all impedance mismatching situations, the extracted Q_i' is very close to Q_i (within 2.0% accuracy), validating our graphical method.

Table 1. The extracted resonance parameters and calculated feedline parameter u from simulations under different impedance mismatching conditions by varying the feedline width. Note that in the last row, we insert two ideal inductors (1 nH, 2 mm long) into the input and output feedline, to simulate the wirebond effects. For comparison, the true resonance parameters are: $f_r = 0.984\,405$ GHz, $Q_c = 17.2 \times 10^3$, $Q_i = 121.9 \times 10^3$ and $Q = 15.1 \times 10^3$.

$w_{in}(\mu$m)	w_{out} (μm)	R_{in}(ohm)	R_{out}(ohm)	u	$Q_i'(10^3)$	$Q_c'(10^3)$	$Q'(10^3)$	f_r' (GHz)
470	470	50	50	$-0.004 - 0.001$i	121.9	17.2	15.1	0.984 405
300	300	65.5	65.5	$-0.096 + 0.003$i	122.0	19.1	16.5	0.984 404
560	560	45	45	$0.073 + 0.003$i	122.1	16.2	14.3	0.984 404
800	800	35.6	35.6	$0.387 + 0.183$i	124.4	12.3	11.3	0.984 399
100	100	116.3	116.3	$0.613 + 0.099$i	122.0	10.7	9.8	0.984 403
100	300	116.3	65.5	$-0.098 - 0.412$i	121.9	17.5	16.6	0.984 415
300	800	65.5	35.6	$0.016 - 0.492$i	121.4	15.3	14.9	0.984 419
470(1 nH)	470(1 nH)	50.4	50.4	$-0.345 - 0.059$i	121.9	26.1	21.6	0.984 406

Table 2. The extracted resonance parameters and calculated feedline parameter u from simulations at different dissipation levels by varying the surface resistance. The impedance mistatching is fixed by setting the width of input and output feedline at 800 μm (refer to corresponding row in table 1).

R_{dc} (ohm/sq)	$Q_i(10^3)$	$Q_c(10^3)$	$Q(10^3)$	u	$Q_i'(10^3)$	$Q_c'(10^3)$	$Q'(10^3)$	f_r'(GHz)
80×10^{-6}	7.6	17.2	5.3	$0.388 + 0.183$i	7.6	12.3	4.7	0.984 399
30×10^{-6}	20.3	17.2	9.3	$0.388 + 0.183$i	20.2	12.3	7.7	0.984 399
10×10^{-6}	61.0	17.2	13.4	$0.388 + 0.183$i	62.9	12.3	10.4	0.984 399
5×10^{-6}	121.9	17.2	15.1	$0.388 + 0.183$i	124.4	12.3	11.3	0.984 399
3×10^{-6}	203.1	17.2	15.9	$0.388 + 0.183$i	199.7	12.3	11.7	0.984 399
1.5×10^{-6}	406.4	17.2	16.5	$0.388 + 0.183$i	399.7	12.3	12.0	0.984 399

We then study the effects of dissipation while fixing impedance mismatching (the width of input and output feedline is fixed at 800 μm). We tune the dc sheet resistance R_{dc} of the metal layer to change dissipation and thus vary Q_i. For instance, we have $Q_i = 121.9 \times 10^3$ for the resonator-coupler block by setting $R_{dc} = 5 \times 10^{-6}$ ohm/sq. Table 2 lists the calculated u and extracted resonance parameters at different dissipation levels. One can see that u, Q_c, Q_c' and f_r' do not change with dissipation. In the internal-Q limit where $Q_c \gg Q_i$, the extracted Q_i' is equal to its true value Q_i. In the coupling-Q limit where $Q_c \ll Q_i$, the extracted Q_i' slightly deviates from Q_i with a deviation less than 1.7%. This is expected, because for very high Q_i approaching or above 10^6, point A (see figure 3(a)) is very close to the origin, which will degrade the signal-to-noise ratio in the data analysis.

4. Experiments

To further test our method, we also analyze a set of transmission data of superconducting microstirp TiN resonators. As shown in figure 5(a), the resonator has a lumped element design with an inter-digitated capacitor (IDC) shunted by an inductive strip. The IDC has 5 μm finger/gap width and a large area $\approx$ 0.9 mm $\times$ 0.9 mm, which is much larger than the inductive strip. The resonator device is made from a 20 nm thick TiN/Ti/TiN trilayer film deposited on a high-resistivity Si substrate. Such TiN resonators were initially developed for feedhorn-coupled MKIDs demonstrating photon-noise limited sensitivity at submillimeter wavelengths [30] and photon-counting MKIDs at telecommunication wavelengths [31]. We place 5 similar resonators on the same chip and couple them to the same 50 ohm microstrip transmission line. All the resonators have identical IDC. We vary the geometry of the inductor strip to create a little frequency difference and the resonance frequency is designed to be in a narrow frequency band of 0.94 ~ 0.96 GHz. The tested device is placed in a magnetically shielded copper box (see figures 5(b) and 2(a)) mounted at 40 mK stage in an adiabatic demagnetization refrigerator (ADR). The magnetic shielding can help reducing the loss due to flux trapping at local sites. The resonator is driven at low microwave excitation power limit and the output signal is amplified by a low noise SiGe amplifier at 4 K before being further amplified by a room temperature amplifier and then measured by a VNA at 300 K.

As shown in figure 5(c), the measured resonance frequencies of the 5 resonators are in the range of 1.05 ~ 1.07 GHz, which are in good agreement with their designed values. Figure 5(d) shows the transmission of one resonator in the complex plane, from which we can extract its experimental resonance parameters. The extracted Q_i' of all the 5 resonators is shown in figure 5(e). One can see that Q_i' is approximately equal for all resonators and fluctuates around 182.5×10^3 within a deviation less than 1.1%. The high consistency of measured Q_i' is reasonable, because all the resonators have identical IDC with a large area. It is believed that at ultra-low temperature and low electric field, the two-level systems (TLSs) on the metallization or substrate coupling to the capacitive parts of the circuits should be the dominant source of loss [32]. Therefore, this result can be considered as an evidence of the success of our graphical method to obtain Q_i'. Note that we also use DCM to extract Q_i' and get the same results,

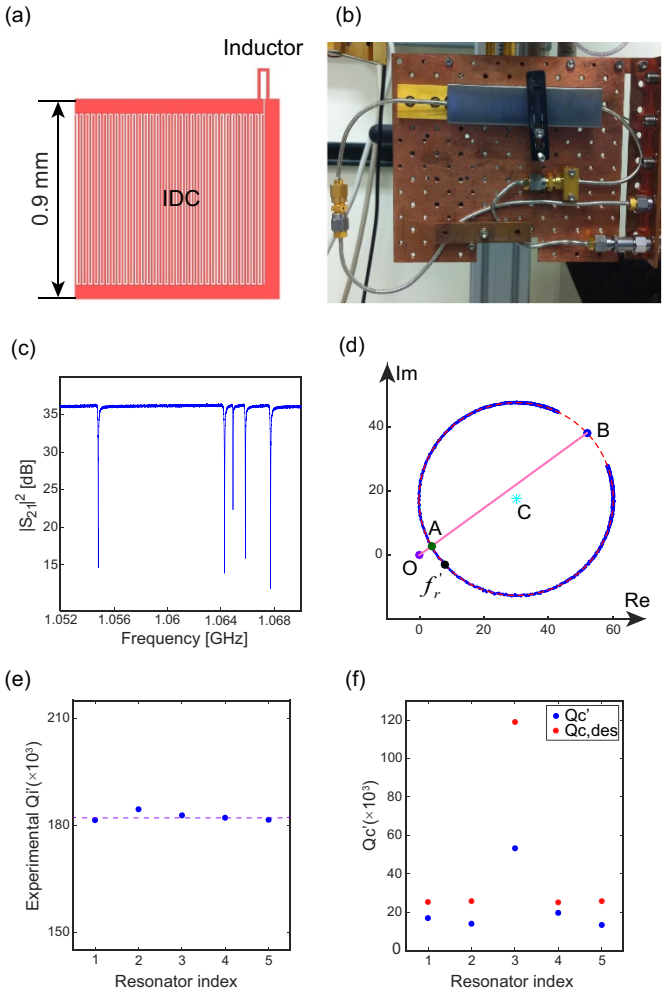

Figure 5. (a) The lumped element design of the tested superconducting TiN resonator. The IDC has a large area about 0.9 mm × 0.9 mm, much larger than inductor strip. (b) Magnetically shielded sample box. (c) Measured $|S_{21}|^2$ and resonance dips. (d) The graphical method to extract Q_i'. The blue circle is the measured transmission at low excitation power, which can be fitted by the red dashed circle using a phase-frequency relation. From fitting, one can obtain the off-resonance point B (blue dot), circle center C (cyan star), resonance frequency f_r' (black dot) and modified total quality factor Q'. The line $|OA|$, where O is origin, cross the transmission circle at point A (green dot). Then Q_i' can be calculated according to equation (9). (e) The extracted Q_i' for all the resonators. (f) The designed Q_c and experimental Q_c' for all the resonators.

confirming the agreement between DCM and our graphical method. Figure 5(f) compares the designed Q_c and experimental Q_c'. The measured Q_c' shows fluctuations, but on average about 40% lower than its designed value. If we assume the designed Q_c is close to its true value, then it is likely that the wire-bond, feedline on PCB, and soldered connectors in this experiment somehow makes $|1+u|$ close to 1.7 and have a little position dependence. This needs more experiments to investigate. Besides, it is worth to note that Res. 2 and 3 are designed to have exactly the same inductor and IDC, but with different designed coupling quality factor $Q_{c,des}$, showing that Q_i' can be accurately extracted for both low and high Q_c situations.

It is also interesting to extract the true Q_c and the feedline parameter u from the measured resonance data. However, equation (6) shows that the modified transmission is defined by 4 independent parameters: Q', Q_c', f_r' and θ. They are insufficient to pin down all the 5 unknown fitting parameters: Q, Q_c, f_r, u_r and u_i (see equation (6)) from only the measured transmission. To get across this problem, one may get more information of u from the background transmission and the reflection S_{11} measurement (see appendix). One also needs to calibrate the transmissions and reflections of the cables before and after the device box in experiments. This is our future research interest.

5. conclusion

In summary, we have developed a 3-block network analysis method to study the effects of impedance mismatched feedline to the superconducting resonance circuits. It is shown that the non-ideal effects of circuits will modify the transmission curve, from which the extracted resonance parameters (particularly Q_c) are different from their true values as originally defined in impedance matched conditions. We show that the extracted resonance parameters are related to their true values by a single feedline parameter u, which includes all the effects from the impedance mismatched feedline. We prove the internal quality factor Q_i can be accurately extracted from the modified transmission curve by using a simple graphical method. These results are quantitatively verified by both simulations and experiments on superconducting TiN resonators. Our method is easy to understand, and provides a general approach to analyze the non-ideal microwave resonant circuits.

Acknowledgment

This work was supported in part by the National Natural Science Foundation of China (Grant Nos. 61871333, 11974290).

appendix: derivation of the *S*-parameter

Here we derive the S-parameter of the 3-block network based on the signal flow graph [28] shown in figure 2(b). We first derive S_{21} by considering the signal flowing from a_1 to b_2, and the simplified signal flow graph is shown in figure A1(a). By using splitting rule at nodes d_1 and c_2, figure A1(a) can be reduced to figure A1(b), where d_1 and c_2 are split into two separate nodes. Figure A1(b) can be further simplified to figure A1(c) by using self-loop rule at nodes c_1 and d_2, and using series rule at nodes d_1 and c_2. Using splitting rule at d_2, figure A1(c) can be reduced to a single branch between two nodes (figure A1(d)), from which the total transmission S_{21} (equation (4)) can be easily obtained.

We then derive the total reflection S_{11} of the 3-block network by considering the signal flowing from a_1 to b_1. The simplified signal flow graph is shown in figure A2.

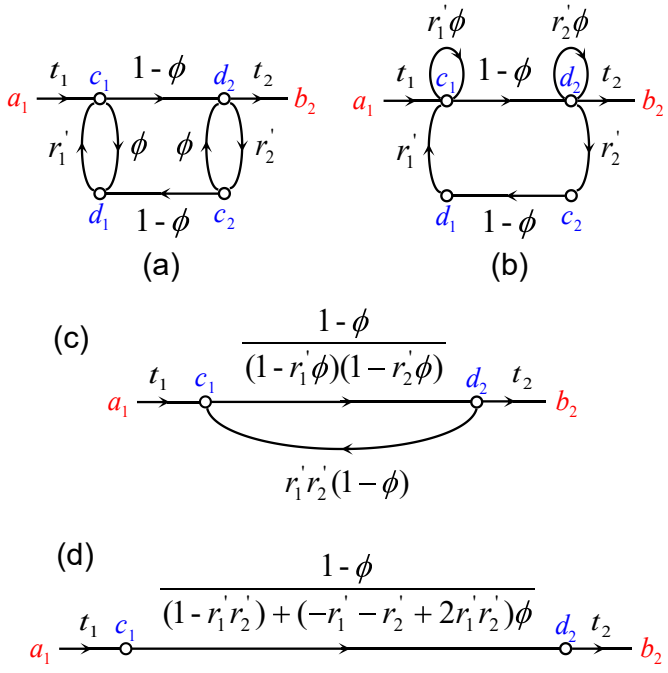

Figure A1. The signal flow graph to derive S_{21} step by step.

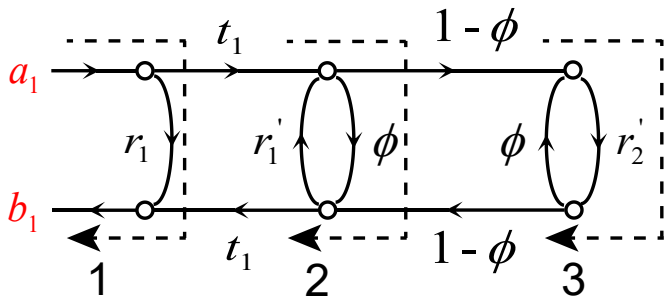

Figure A2. The signal flow graph to derive S_{11}.

One can see that there are 3 signal flow paths contributing to reflection. The first path directly gives $S_{11}(1) = r_1$. After a little math and neglecting higher order terms like $(1-\phi)^2 r_1' r_2'$, one can also work out the reflection from the second path and third path, which are $S_{11}(2) = \frac{t_1^2\phi}{1-r_1'\phi}$ and $S_{11}(3) = \frac{t_1^2(1-\phi)^2 r_2'}{1-r_1'r_2'+(-r_1'-r_2'+2r_1'r_2')\phi}$. By using the parallel rule of signal flow graph, the total reflection is equal to the sum of $S_{11}(1)$, $S_{11}(2)$ and $S_{11}(3)$. Therefore we have:

$$S_{11} = r_1 + \frac{t_1^2\phi}{1-r_1'\phi} + \frac{t_1^2(1-\phi)^2 r_2'}{(1-r_1'r_2')+(-r_1'-r_2'+2r_1'r_2')\phi} \tag{A1}$$

ORCID iD

Y Wang https://orcid.org/0000-0003-2337-1181

References

[1] Zmuidzinas J 2012 *Annu. Rev. Condens. Matter Phys.* **3** 169
[2] Day P K, LeDuc H G, Mazin B A, Vayonakis A and Zmuidzinas J 2003 *Nature* **425** 817
[3] Wallraff A, Schuster D I, Blais A, Frunzio L, Huang R S, Majer J, Kumar S, Girvin S M and Schoelkopf R J 2004 *Nature* **431** 162C167
[4] Houck A *et al* 2008 *Phys. Rev. Lett.* **101** 1
[5] Eom B H, Day P K, LeDuc H G and Zmuidzinas J 2012 *Nature* **8** 623
[6] Chaudhuri S, Li D, Irwin K D, Bockstiege C, Hubmayr J, Ullom J N, Vissers M R and Gao J 2017 *Appl. Phys. Lett.* **110** 152601
[7] Mazin B 2004 *Ph.D. thesis* Caltech
[8] Doyle S, Mauskopf P, Naylon J, Porch A and Duncombe C 2008 *J Low Temp Phys* **151** 550
[9] Paiella A *et al* 2019 *JCAP* **1** 039
[10] Barends R, Baselmans J, Hovenier J, Gao J, Yates S, Klapwijk T and Hoevers H 2007 *IEEE Trans. Appl. Supercond* **17** 263
[11] Vissers M, Gao J, Wisbey D, Hite D, Tsuei C C, Corcoles A, Steffen M and Pappas D 2010 *Appl. Phys. Lett.* **97** 232509
[12] Megrant A *et al et al* 2012 *Appl. Phys. Lett.* **100** 113510
[13] OConnell A *et al* 2008 *Appl. Phys. Lett.* **92** 112903
[14] Barends R, Vercruyssen N, Endo A, Visser P, Zijlstra T, Klapwijk T, Diener P, Yates S and Baselmans J 2010 *Appl. Phys. Lett.* **97** 023508
[15] Wisbey D, Gao J, Vissers M, Silva F, Kline J, Vale L and Pappas D 2010 *Appl. Phys. Lett.* **108** 093918
[16] Budoyo R P, Hertzberg J B, Ballard C J, Voigt K D, Kim Z, Anderson J R, Lobb C J and Wellstood F C 2016 *Phys. Rev.* B **93** 024514
[17] Grunhaupt L *et al* 2018 *Phys. Rev. Lett.* **121** 117001
[18] Burnett J, Faoro L and Lindstrom T 2016 *Supercond. Sci. Technol.* **29** 044008
[19] Deng C, Otto M and Lupascu A 2013 *J. Appl. Phys* **114** 054504
[20] Kajfez D 1995 *IEE Proc. Microwaves Antennas Propag.* **142** 369
[21] Petersan P J and Anlage S M 1998 *J. Appl. Phys* **84** 3392
[22] Leong K and Mazierska J 2002 *IEEE Trans. Microwave Theory Tech* **50** 2115
[23] Khalil M S, Stoutimore M J A, Wellstood F C and Osborn K D 2012 *J. Appl. Phys* **111** 054510
[24] Paika H and Osborn K D 2010 *Appl. Phys. Lett.* **96** 072505
[25] Probst S, Song F, Bushev P, Ustinov A and Weides M 2015 *Rev. Sci. Instrum.* **86** 024706
[26] Gao J 2008 *Ph.D. thesis* Caltech
[27] Noroozian O 2012 *Ph.D. thesis* Caltech
[28] Pozar D 2009 *Microwave Engineering* (New York: Wiley)
[29] Richardson C, Siwak N, Hackley J, Keane Z, Robinson J, Arey B, Arslan I and Palmer B 2016 *Supercond. Sci. Technol.* **29** 064003
[30] Hubmayr J *et al* 2015 *Appl. Phys. Lett.* **106** 073505
[31] Guo W *et al* 2017 *Appl. Phys. Lett.* **110** 212601
[32] Vissers M, Weides M, Kline J, Sandberg M and Pappas D 2012 *Appl. Phys. Lett.* **101** 022601